*Int. J. Electrochem. Sci.*, 15 **(2020)** 10375 – 10381, doi: 10.20964/2020.10.11

International Journal of
ELECTROCHEMICAL
SCIENCE
www.electrochemsci.org

*Short Communication*

# Intermediate Temperature Electrochemical Properties of $Sn_{0.95}Ni_{0.05}P_2O_7/KPO_3$ Composite Electrolyte

*Guoquan Shao, Lili Wang, Wenjian Wang, Qingxin Guo, Hui Zhu, Jilong Ma*[*]

Traditional Chinese Medicine College, Bozhou University, Bozhou 236800, Anhui, China
[*]E-mail: bzxymjl2019@163.com

*Received:* 22 May 2020 / *Accepted:* 26 July 2020 / *Published:* 31 August 2020

In this study, a pyrophosphate-based composite electrolyte of $Sn_{0.95}Ni_{0.05}P_2O_7/KPO_3$ was prepared by a solid state method. The structure and electrical properties of the composite were studied using X-ray diffractometer, electrochemical workstation etc. XRD test showed that $Sn_{0.95}Ni_{0.05}P_2O_7$ maintains the original lattice structure and does not react with $KPO_3$ phase. The results show the sample was an ionic conductor in the high oxygen partial pressure range and was a mixed conductor of ions and electrons in the low oxygen partial pressure range. The highest power output density and conductivity of $Sn_{0.95}Ni_{0.05}P_2O_7/KPO_3$ were 64.2 $mW \cdot cm^{-2}$ and $2.4 \times 10^{-2}$ $S \cdot cm^{-1}$ at 700 °C, respectively.

**Keywords:** Composite; Pyrophosphate; Electrolyte; Fuel cell; Conductivity

## 1. INTRODUCTION

Energy crises and environmental pollution are two major problems for the sustainable development of modern society. The search for efficient and environmentally friendly energy conversion technologies has become a focus around the world, and fuel cell technology is regarded as one of the most promising technologies [1–3]. A fuel cell includes an electrolyte, sealing material, cathode, anode and connecting material. However, the high operating temperature of fuel cells is the key factor limiting their development. Reducing operating temperature is the primary problem in fuel cell research [4–7].

The operating temperature of fuel cells is mainly affected by the ionic conductivity of the electrolyte [8–11]. In recent years, pyrophosphate-based ($MP_2O_7$, M = Sn, Ti and Ce) electrolyte materials with high conductivities at 150–350 °C have been developed [12–17]. Hibino et al. investigated $In^{3+}$, $Al^{3+}$ and $Mg^{2+}$ doped $SnP_2O_7$ and found that their conductivities were higher than $10^{-2}$ $S \cdot cm^{-1}$ at 150–300 °C [12–14].

To improve the ionic conductivities, composite electrolytes have been widely studied [18–22]. Hibino et al. synthesized a novel composite electrolyte of $H_3PO_4$-doped

polybenzimidazole/$Sn_{0.95}Al_{0.05}P_2O_7$ [18]. Shi and Wang et al. reported that $Sn_{0.95}Al_{0.05}P_2O_7$/ $KSn_2(PO_4)_3$ composite electrolyte had good intermediate temperature electrical properties at 400-700 °C [22]. Nickel salt is abundant, cheap and has the same radius as tin. Therefore, $Sn_{0.95}Ni_{0.05}P_2O_7/KPO_3$ composite electrolyte was synthesized in this study. The structure was characterized by Raman spectrometer and X-ray diffractometer. The intermediate temperature (400–700 °C) electrochemical properties were also investigated through the relationship between oxygen partial pressure and conductivity, and conductivity and fuel cell test.

## 2. EXPERIMENTAL

$Sn_{0.95}Ni_{0.05}P_2O_7/KPO_3$ was synthesized by a solid state method. All reagents used in this study were of analytical grade. 2.7642 g $K_2CO_3$, 8.5905 g $SnO_2$, 0.5481 g $Ni(NO_3)_2$ and 11 mL 85 % $H_3PO_4$ were fully milled and heated at 400 °C for 1 h to react preliminary. After cooling, they were taken out and ground into powders. The powders were pressed by a tablet press under 300 MPa and calcined at 500 °C and 700 °C for 1 h, respectively, to obtain a composite electrolyte sheet with a diameter of 18 mm and a thickness of 1.1 mm.

The structure of $Sn_{0.95}Ni_{0.05}P_2O_7/KPO_3$ was characterized by X-ray diffractometer (X'pert Pro MPD) and Raman spectrometer (invia). The Pd-Ag slurry was coated on both sides of the composite electrolyte to remove the organic matter at 600 °C and obtain a uniform collector. The conductivities of $Sn_{0.95}Ni_{0.05}P_2O_7/KPO_3$ in a nitrogen atmosphere were measured by the three-electrode AC impedance method from 1 to $10^5$ Hz at 400–700 °C. The relationship between oxygen partial pressure and conductivity was also investigated. Finally, an $H_2/O_2$ fuel cell was assembled to study the discharge performance of $Sn_{0.95}Ni_{0.05}P_2O_7/KPO_3$.

## 3. RESULTS AND DISCUSSION

Fig. 1 shows the XRD spectra of $Sn_{0.95}Ni_{0.05}P_2O_7/KPO_3$ composite and pure $SnP_2O_7$ powder. In the composite electrolyte, the $Sn_{0.95}Ni_{0.05}P_2O_7$ phase maintains its original structure. And the positions of characteristic peaks are consistent with the standard spectrum of pure $SnP_2O_7$. $KPO_3$ mainly exists in an amorphous state with a weak diffraction peak at 26.35° [22]. Besides, there are weak diffraction peaks of $SnO_2$ at 26.72° and 33.98°. In the synthesis process, the following reaction of $SnP_2O_7 + K_2CO_3 = SnO_2 + 2KPO_3 + CO_2\uparrow$ may cause the appearance of $SnO_2$. $Sn_{0.95}Ni_{0.05}P_2O_7$ maintains the original lattice structure and does not react with $KPO_3$ phase, which shows that $Sn_{0.95}Ni_{0.05}P_2O_7$ particles have good anti metaphosphate corrosion ability [23].

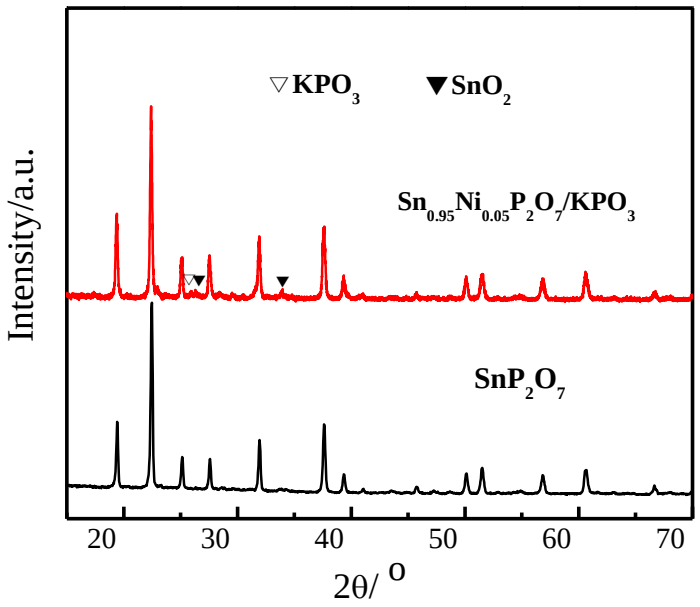


**Figure 1.** XRD results of $SnP_2O_7$ and $Sn_{0.95}Ni_{0.05}P_2O_7/KPO_3$ composite.

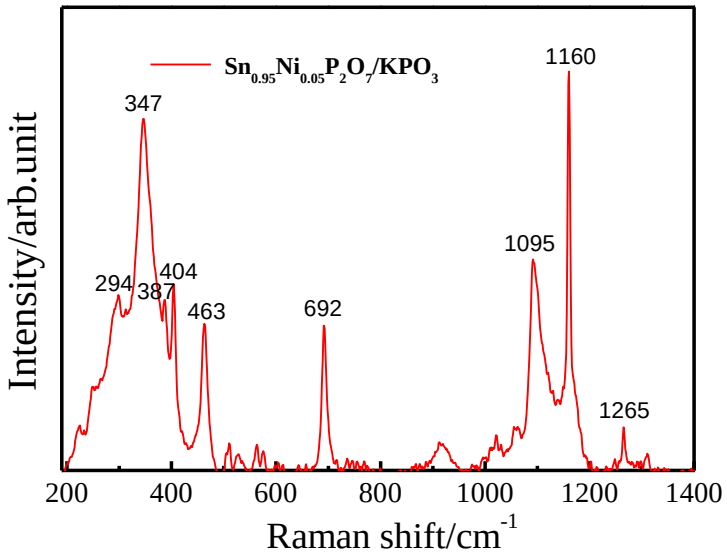


**Figure 2.** Raman results of $Sn_{0.95}Ni_{0.05}P_2O_7/KPO_3$ composite.

The Raman results of $Sn_{0.95}Ni_{0.05}P_2O_7/KPO_3$ are shown in Fig. 2. A broad peak below 410 $cm^{-1}$ belongs to the $PO_4$ tetrahedron (pyrophosphate) bending vibration. There is a new vibration peak near 463 $cm^{-1}$, which may be attributed to K-O-P vibration. The bands at 692 $cm^{-1}$, 1160 $cm^{-1}$ and 1265 $cm^{-1}$ are P-O-P symmetric, $(PO_2)$- symmetric and $(PO_2)$- asymmetric (metaphosphate) stretching vibration, respectively [24]. The Raman results further illustrate that $Sn_{0.95}Ni_{0.05}P_2O_7$ is the main component, and $KPO_3$ exists simultaneously (see also Fig. 1).

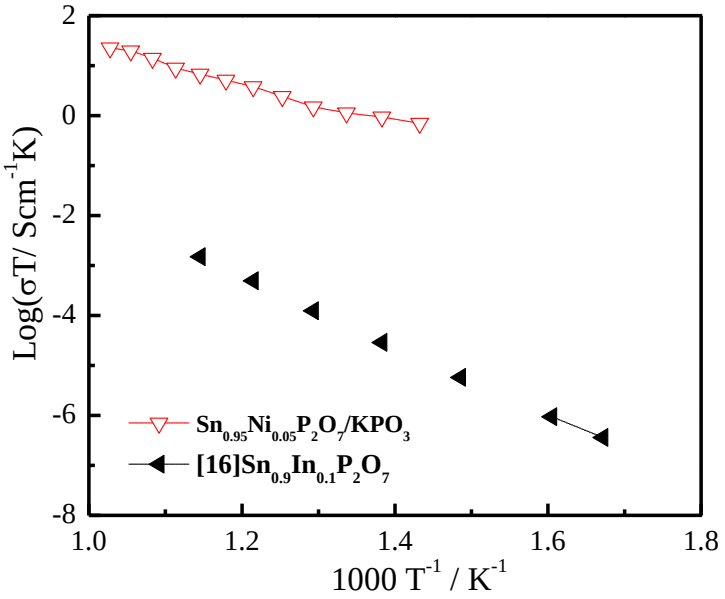


**Figure 3.** The conductivities of $Sn_{0.95}Ni_{0.05}P_2O_7/KPO_3$ in a nitrogen atmosphere at 400–700 °C.

Fig. 3 shows the conductivity test results of $Sn_{0.95}Ni_{0.05}P_2O_7/KPO_3$ in a nitrogen atmosphere at 400–700 °C. The conductivities of $Sn_{0.95}Ni_{0.05}P_2O_7/KPO_3$ increase significantly, while the activation energy decreases. The highest conductivities of $Sn_{0.95}Ni_{0.05}P_2O_7/KPO_3$ reach $7.8\times10^{-3}$ and $2.4\times10^{-2}$ $S\cdot cm^{-1}$ at 600 °C and 700 °C, respectively, which are markedly higher than $Sn_{0.9}In_{0.1}P_2O_7$ ($1.7\times10^{-6}$ $S\cdot cm^{-1}$ at 600 °C). In the composite electrolyte, in addition to the $KPO_3$ phase, the $Sn_{0.95}Ni_{0.05}P_2O_7$ bulk phase is also an important way of proton and oxide ionic conduction [22–24]. Therefore, ions can be conducted through the metaphosphate phase, and also through the interface between ceramic bulk phase and $KPO_3$ phase.

Fig. 4 shows the relationship between oxygen partial pressure and conductivity of $Sn_{0.95}Ni_{0.05}P_2O_7/KPO_3$ at 700 °C. In a certain range of oxygen partial pressure, if $\log \sigma \sim \log (pO_2)$ is in a horizontal linear relationship, the sample shows ionic conductivity. If $\log \sigma \sim \log (pO_2)$ is in a non-horizontal linear relationship, the sample shows mixed conductivity of ions and electrons (or holes) [25]. It can be seen from Fig. 4 that the conductivity is not affected by the oxygen partial pressure within the range of high oxygen partial pressure ($pO_2 = 10^{-5} \sim 10^{0}$ atm), indicating that the sample is an ionic conductor. In the range of low oxygen partial pressure ($pO_2 = 10^{-20} \sim 10^{-15}$ atm), the conductivity increases with the decrease of oxygen partial pressure, indicating that the sample is a mixed conductor of ions and electrons.

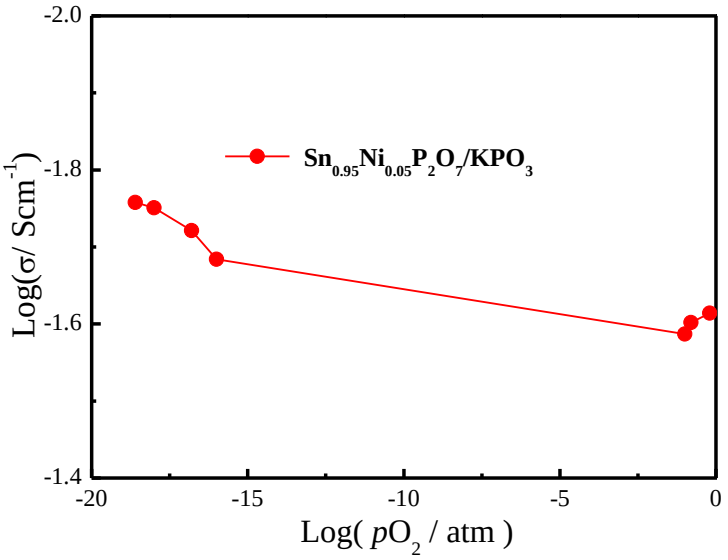


**Figure 4.** The relationship between oxygen partial pressure and conductivity of $Sn_{0.95}Ni_{0.05}P_2O_7/KPO_3$ at 700 °C.

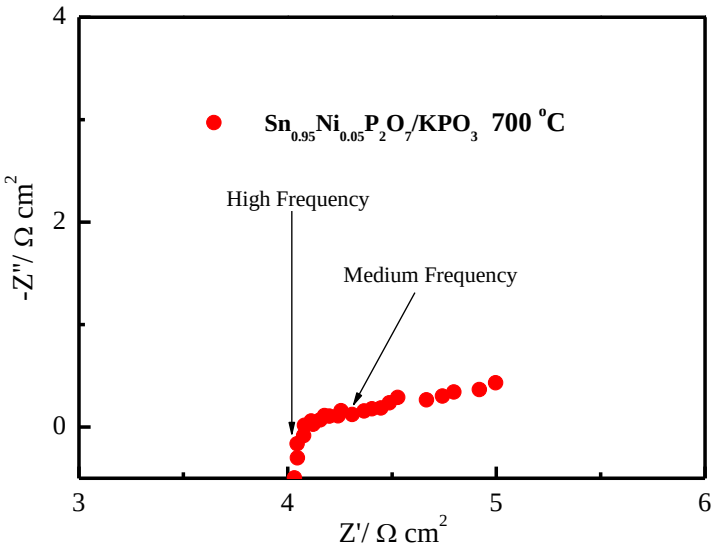


**Figure 5.** AC impedance spectrum of $Sn_{0.95}Ni_{0.05}P_2O_7/KPO_3$ under open circuit condition.

A typical AC impedance spectrum is shown in Fig. 5. The intersection at the end of the real axis (high frequency) represents the electrolyte resistance (4.08 $\Omega \cdot cm^2$). The grain boundary process of $Sn_{0.95}Ni_{0.05}P_2O_7/KPO_3$ corresponds to medium frequency (4.66 $\Omega \cdot cm^2$). The difference between them corresponds to polarization resistance (0.58 $\Omega \cdot cm^2$).

The $H_2/O_2$ fuel cell discharge performance of $Sn_{0.95}Ni_{0.05}P_2O_7/KPO_3$ at 700 °C is shown in Fig. 6. The open circuit voltage (1.04 V) is lower than the theoretical value (1.12 V) because the part of $Sn^{4+}$ is reduced to $Sn^{2+}$ in a high temperature reducing atmosphere, resulting in electronic conduction and short circuit in the cell [23–24]. The highest power output density of $Sn_{0.95}Ni_{0.05}P_2O_7/KPO_3$ is 64.2 $mW \cdot cm^{-2}$ at 700 °C. It can be seen that the electronic conduction in a reducing atmosphere is an important reason for its low performance in a fuel cell. The power output of ours is lower than those of

$Sn_{0.9}Cu_{0.1}P_2O_7/KPO_3$ [26] and $Sn_{0.9}Ni_{0.1}P_2O_7/KPO_3$ [27], however, it is equivalent to $Sn_{0.95}Ga_{0.05}P_2O_7/KPO_3$ [23] under the same conditions (Table 1). This can be ascribed to the oxygen vacancy concentrations of 10 mol% $M^{n+}$ doped $SnP_2O_7/KPO_3$ being much higher than those 5 mol% samples. The inhibition of $KPO_3$ on electron conduction is not obvious. Only when the chemical stability is improved, can these substances be used in fuel cells.

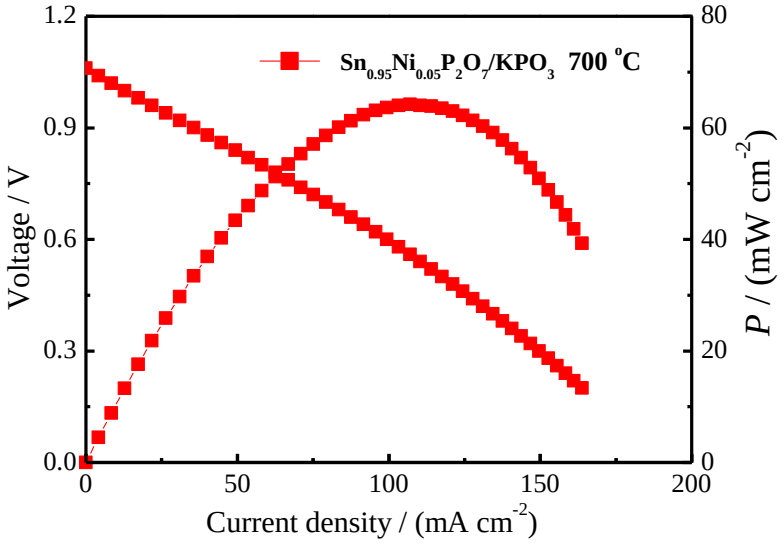


**Figure 6.** The discharge performance of $Sn_{0.95}Ni_{0.05}P_2O_7/KPO_3$ at 700 °C.

**Table 1.** The highest power densities of $Sn_{0.95}Ni_{0.05}P_2O_7/KPO_3$ and similar electrolytes in the literatures.

| electrolytes | Highest power densities |
|---|---|
| $Sn_{0.95}Ni_{0.05}P_2O_7/KPO_3$ | 64.2 mW·cm$^{-2}$, 700 °C, this work |
| $Sn_{0.9}Cu_{0.1}P_2O_7/KPO_3$ | 131 mW·cm$^{-2}$, 700 °C, [26] |
| $Sn_{0.9}Ni_{0.1}P_2O_7/KPO_3$ | 434 mW·cm$^{-2}$, 700 °C, [27] |
| $Sn_{0.95}Ga_{0.05}P_2O_7/KPO_3$ | 87 mW·cm$^{-2}$, 700 °C, [23] |

## 4. CONCLUSIONS

In this study, $Sn_{0.95}Ni_{0.05}P_2O_7/KPO_3$ was prepared by a solid state method. The Raman results illustrated that $Sn_{0.95}Ni_{0.05}P_2O_7$ is the main component, and $KPO_3$ exists simultaneously. The highest conductivities of $Sn_{0.95}Ni_{0.05}P_2O_7/KPO_3$ reached $7.8\times10^{-3}$ and $2.4\times10^{-2}$ S·cm$^{-1}$ at 600 °C and 700 °C, respectively. The polarization resistance of $Sn_{0.95}Ni_{0.05}P_2O_7/KPO_3$ under an open circuit condition reached 0.58 Ω·cm$^2$ at 700 °C. The highest power output density of $Sn_{0.95}Ni_{0.05}P_2O_7/KPO_3$ was 64.2 mW·cm$^{-2}$ at 700 °C.

ACKNOWLEDGEMENTS
This work was supported by the Natural Science Project of Anhui Province (No. KJ2019A1304), High level teaching team of Anhui Provincial Department of Education (No. 2018jxtd079).

CONFLICTS OF INTEREST
The authors declare no conflicts of interest.

**References**

1. Y. Yang, H. Hao, L. Zhang, C. Chen, Z. Luo, Z. Liu, Z. Yao, M. Cao and H. Liu, *Ceram. Int.*, 44 (2018) 11109.
2. Y. Tian, Z. Lü, X. Guo and P. Wu, *Int. J. Electrochem. Sci*., 14 (2019) 1093.
3. C. Xia, Z. Qiao, C. Feng, J. Kim, B. Wang and B. Zhu, *Materials*, 11(2018) 40.
4. X. Fang, J. Zhu and Z. Lin, *Energies*. 11 (2018) 1735.
5. Z. Zhang, L. Chen, Q. Li, T. Song, J. Su, B. Cai, H. He, *Solid State Ionic*s, 323 (2018) 25.
6. A.A. Solovyev, S.V. Rabotkin, A.V. Shipilova and I.V. Ionov, *Int. J. Electrochem. Sci*., 14 (2019) 575.
7. W. Wang, D. Medvedev and Z. Shao, *Adv. Funct. Mater.*, (2018) 1802592.
8. H. Jiang and F. Zhang, *Int. J. Electrochem. Sci*., 15 (2020) 959.
9. W. Wang, D. Medvedev and Z. Shao, *Adv. Funct. Mater.*, 2018, 1802592.
10. S.H. Morejudo, R. Zanón, S. Escolástico, I. Yuste-Tirados, H. Malerød-Fjeld, P.K. Vestre, W.G. Coors, A. Martínez, T. Norby, J.M. Serra and C. Kjølseth, *Science,* 353 (2016) 563.
11. G. Yang and S.-J. Park, *Materials*, 12 (2019) 1177.
12. A. Tomita, N. Kajiyama, T. Kamiya, M. Nagao and T. Hibino, *J. Electrochem. Soc.*, 154 (2007) B1265.
13. M. Nagao, T. Kamiya, P. Heo, A. Tomita, T. Hibino and M. Sano, *J. Electrochem. Soc.*, 153 (2006) A1604.
14. K. Genzaki, P. Heo, M. Sano and T. Hibino, *J. Electrochem.Soc.*, 156 (2009) B806.
15. H Wang, L Sun, J Chen and C Luo, *Acta Phys.-Chim. Sin.*, 28 (2012) 2893.
16. S.R. Phadke, C.R. Bowers, E.D. Wachsman and J.C. Nino, *Solid State Ionics*, 183 (2011) 26.
17. S. Tao, *Solid State Ionics*, 180 (2009) 148.
18. Y.C. Jin, M. Nishida, W. Kanematsu and T. Hibino, *J. Power Sources*, 196 (2011) 6042.
19. Y. Sato, Y.B. Shen, M. Nishida, W. Kanematsu and T. Hibino, *J. Meter. Chem.*, 22 (2012) 3973.
20. B. Singh, A. Bhardwaj, S. K. Gautam, D. Kumar, O. Parkash, I.-H. Kim and S.-J. Song, *J. Power Sources*, 345 (2017) 176.
21. Y. Jin and T. Hibino, *Electrochim. Acta,* 55 (2010) 8371.
22. J. Liu, R. Du, R. Shi and H. Wang, *Ceram. Int.*, 44 (2018) 5179.
23. Y. Han, J. Zhu, P. Sun, N. Wang, *Int. J. Electrochem. Sci*., 15 (2020) 5255.
24. P. A. Bingham and R. J. Hand, *Mater. Res. Bull.*, 43 (2018) 1679.
25. R. M. C. Marques, F. M. B. Marques and J. R. Frade, *Solid State Ionics*, 73 (1994) 15.
26. L. Zhang, W. Chen and W. Hu, *Int. J. Electrochem. Sci*., 15 (2020) 4447.
27. Q. Guan, T. Hu, H. Wang and G. Xi, *Ceram. Int.*, 46 (2020) 11602.